Citrate provides essential disorder for bone mineral

Erika Davies[1], Karin H Muller[2], Chris J. Pickard[3], David G. Reid[1], Jeremy N Skepper[2] and Melinda J Duer[1]

[1]Department of Chemistry, University of Cambridge, Lensfield Road, Cambridge CB2 1EW, UK [2]Department of Physiology, Development and Neuroscience, Downing Street, Cambridge CB2 3DY, UK [3] Department of Physics & Astronomy, University College London, Gower St, London, WC1E 6BT, U.K

Submitted to Proceedings of the National Academy of Sciences of the United States of America

We provide evidence that citrate anions are included within the bone mineral crystal lattice and hypothesize that its presence acts to introduce disorder into the bone mineral atomic structure. In order to assess this hypothesis, we take as a model for a citrate-containing, hydrated calcium phosphate, a double salt, octacalcium phosphate citrate (OCP-cit). We use a combination of multinuclear solid-state NMR, powder X-ray diffraction and first-principles electronic structure calculations in order to propose a quantitative structure for this material, in which citrate anions reside in a hydrated layer, bridging between apatitic layers. In order to assess the relevance of such a structure in native bone mineral, we present for the first time 17O NMR data on bone and compare with 17O NMR data for octacalcium phosphate-citrate and other calcium phosphate minerals relevant to bone. The proposed structural model for bone mineral explains a number of known structural features of bone mineral: the thinness of the mineral platelets, the presence of strongly bound water molecules and the relatively high concentration of hydrogen phosphate compared to orthophosphate. We suggest that disorder in bone mineral is essential in order to limit the disordering of the surrounding organic matrix in bone that must occur upon ordered mineral crystal formation and that the incorporation of citrate into the crystal structure of bone mineral provides a simple mechanism to introduce disorder into the atomic structure.

bone mineral | octacalcium phosphate | citrate | solid-state NMR | NMR crystallography

Introduction

The presence of citrate in bone is an accepted fact. Its association with bone mineral was demonstrated in 2010 (1) by solid-state NMR, but while there are many hypotheses as to its role, there is little evidence to date to confirm or deny any of these ((1) and see Supplementary Information – text, for other references). Here we propose a role for citrate as a means by which the degree of crystallinity or order in bone mineral is controlled. We present detailed characterization of a model compound, octacalcium phosphate citrate to understand how it could perform this role.

Bone is a complex organic-inorganic composite (2) with inorganic mineral nanoparticles held within a primarily collagen protein matrix. Bone mineral is widely believed to form initially from an amorphous calcium phosphate (ACP) phase within the organic matrix, which then re-organises into a crystalline lattice (3). Key is the fact that formation of an *ordered* mineral phase from ACP results in a significant decrease in entropy. In order that the second law of thermodynamics is not contravened, there must be a compensating *increase* in entropy in the surroundings in thermal contact with the bone mineral particles, namely the collagen matrix and surrounding water. However, increasing the entropy or disorder in the collagen matrix is an inherently random and uncontrolled process, undesirable in a system where order in the collagen matrix is required for both molecular and cellular recognition.

Thus the mineralising system needs to be able to control or at least limit the entropy change upon mineral formation so as to prevent potentially pathological disruption of the organic matrix. Significant reduction in the entropy change upon mineral formation can only come about by reducing the atomic order in the final mineral particles. In other words, the mineral particles themselves need the feature of being able to contain a degree of disorder. Solid-state NMR certainly suggests some structural disorder in bone mineral nanocrystals (4, 5), and powder X-ray diffraction studies often describe bone mineral as poorly crystalline (2, 6) so that disorder is present in bone mineral crystals is not in question. More interestingly, there are many biomechanical studies (7–10) that show that the degree of crystallinity of the mineral phase is of critical importance in determining the strength of the bone tissue (rather than, for instance the degree of mineralization), with *increases* in crystallinity associated with impairment in mechanical function (7). These finding together strongly suggests at least some degree of control over the degree of disorder in the bone mineral atomic structure. The key question then becomes, what is the mechanism by which the degree of disorder in the mineral phase is controlled? The answer is central to understanding bone strength and osteodegenerative diseases such as osteoporosis.

With this question in mind, we propose here a new model for bone mineral in which citrate ions reside within the mineral lattice; the ability of the citrate anion to coordinate to surrounding calcium ions via any or all of its one hydroxyl and three carboxylate groups allows it to adopt many possible orientations. In our model, the citrate ions reside within hydrated layers in the mineral crystals so that the citrate ion adopting different orientations or conformations merely requires the re-positioning of relatively mobile water molecules, and thus does not require substantial re-ordering of the crystal lattice. Therefore, it is likely that there are different citrate orientations/ conformations with relatively similar energies that can all be populated at biological temperatures – in other words, a naturally-arising disorder within the atomic structure of the crystal lattice. In order to provide

Significance

Bone contains ∼2% wt citrate, however its role in bone remains a much-debated question. We provide evidence that citrate anions reside within the bone mineral crystal lattice and hypothesize that it acts to introduce disorder into the mineral atomic structure. The Second Law of Thermodynamics states that the entropy of the Universe can only increase. Thus, formation of an ordered mineral crystal lattice (decrease in entropy) must be accompanied by at least an equivalent increase in entropy (disorder) in the surroundings in thermal contact with the mineral crystals, namely the organic matrix. We suggest disorder in bone mineral is essential in order to limit the disordering of the surrounding organic matrix in bone upon formation of mineral crystals.

Reserved for Publication Footnotes

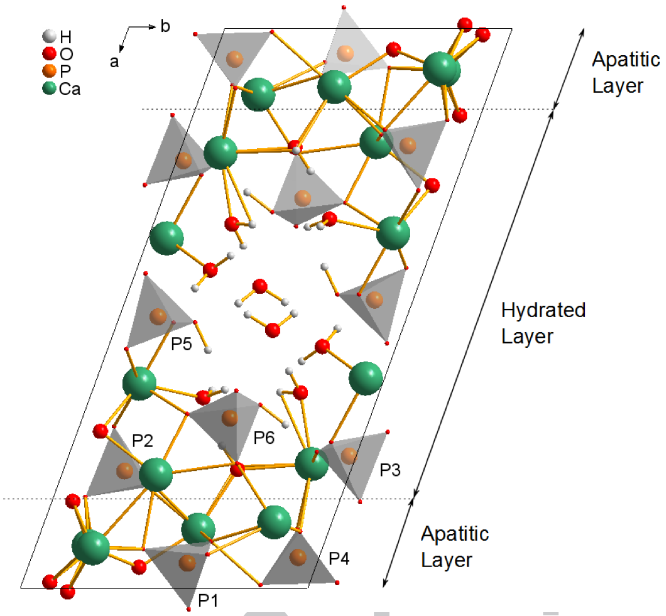

Fig. 1. Powder XRD diffractograms of OCP (red) and OCP-citrate (blue). The shift of the (100) reflection from 4.85° to 4.09° between OCP and OCP-citrate, respectively, is indicative of the expansion of the OCP unit cell along the *a*-axis resulting from incorporation of the citrate within the hydrated layer of OCP. The principal reflections for OCP are labelled; other signals consist of a superposition of several reflections.

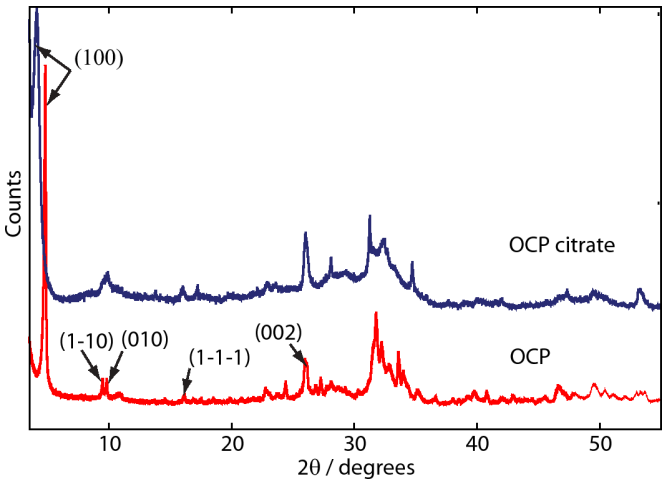

Fig. 2. **(a)** the ^{13}C CP spectrum of OCP-citrate, and **(b)** the ^{13}C Bloch decay spectrum of OCP-citrate (contact time 1 ms). **(c)** The ^{13}C CP spectrum of Ca(Hcitrate).4H_2O (contact time 3 ms) is included for comparison. The signals are labelled as discussed in the text and with the chemical shift at the maximum intensity of the signal.

a model for such a structure, we explore in detail the characteristics of a double salt, octacalcium phosphate-citrate (OCP-citrate) and propose for the first time a quantitative structure for this material using a combination of solid-state NMR spectral parameters, powder X-ray diffraction data and first principles electronic structure calculations.

The existence of OCP-dicarboxylic acid and OCP-tricarboxylic acid double salts was first demonstrated in 1983 (11–13), with a the structural formula of $Ca_{16}(HPO_4)_{2.8}(PO_4)_8(CIT)_{0.8}.16.4\ H_2O$, where CIT corresponds to the 3- anion, proposed for the OCP-citrate double salt on the basis of chemical analysis, with similar formulae for all other double salts characterized, albeit with varying water contents

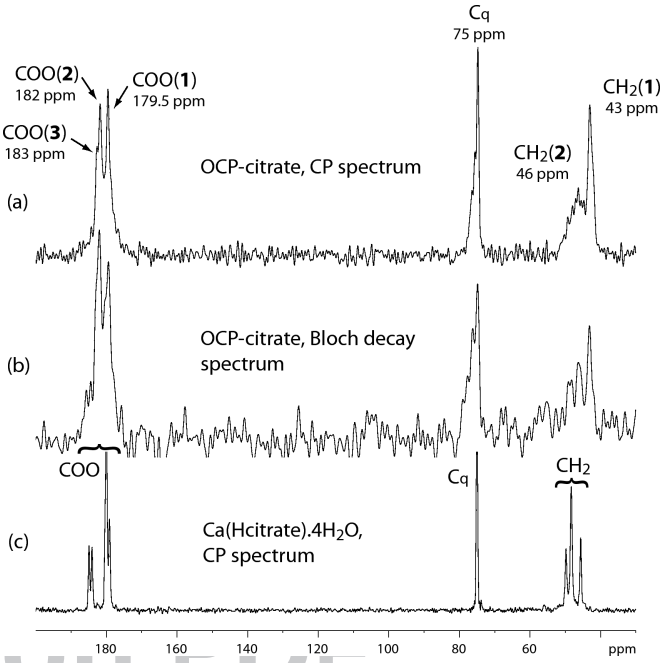

Fig. 3. Comparison of ^{13}C CP MAS spectra of OCP-citrate recorded at 298 K (blue) and 200 K (red) (MAS rate 12 kHz, 2 ms contact time).

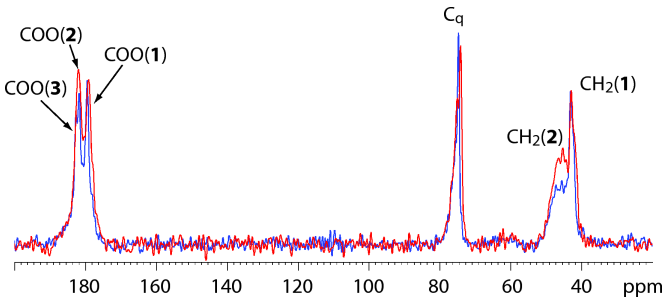

Fig. 4. Top: ^{31}P Bloch decay (BD) MAS spectrum of OCP-citrate; bottom: Bloch decay spectrum of OCP for comparison, with assignments as previously determined (25) using the nomenclature for the phosphorus sites given in Figure 1.

(14). Subsequently, these double salt compounds were shown to have crystallographic structures similar to the parent OCP structure (Fig 1) by powder XRD (14, 15); in all cases, the unit cell of the double salt was shown to be expanded along the *a*-axis, whilst the *b* and *c* unit cell dimensions remained largely unchanged, leading to the proposal that the organic acid anions were incorporated in the (100) plane. According to the composition formula, the organic acid anion replaces one of the hydrogen phosphate sites in the OCP structure, i.e. one of the P5 or P6 sites in the OCP structure shown in Fig 1. Studies of the double salt structures by FT-IR spectroscopy led to the conclusion that it is one of the P5 hydrogen phosphate sites that is replaced by the organic acid anion, because the vibrational bands from this hydrogen phosphate site were significantly attenuated (16, 17) in the double salts, whilst those from the P6 hydrogen phosphate site were relatively undisturbed, a conclusion borne out by a recent detailed, multinuclear NMR study on the OCP-succinate double salt (18).

However, despite this previous work, no quantitative structure has yet been proposed for any of the OCP double salts. In the case of OCP-citrate structure, this is primarily because, from its powder XRD pattern (14), it contains significant disorder or

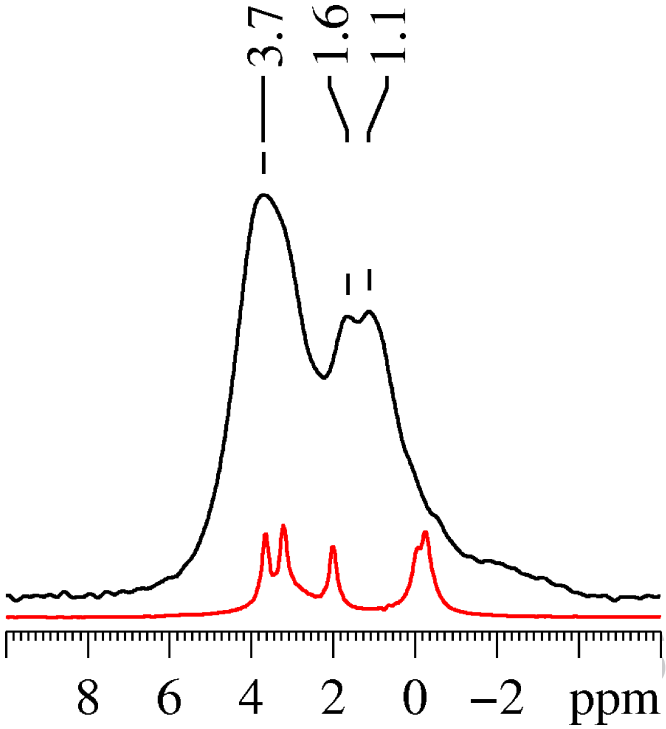

Fig. 5. (top) ^{13}C BD spectra of OCP-citrate (red) and OCP-citrate after being partially dehydrated over P_2O_5 under vacuum for two days (blue). (bottom) ^{13}C CP spectra (contact time 4 ms) of OCP-citrate (red) and OCP-citrate after being dehydrated over P_2O_5 under vacuum for two days (blue).

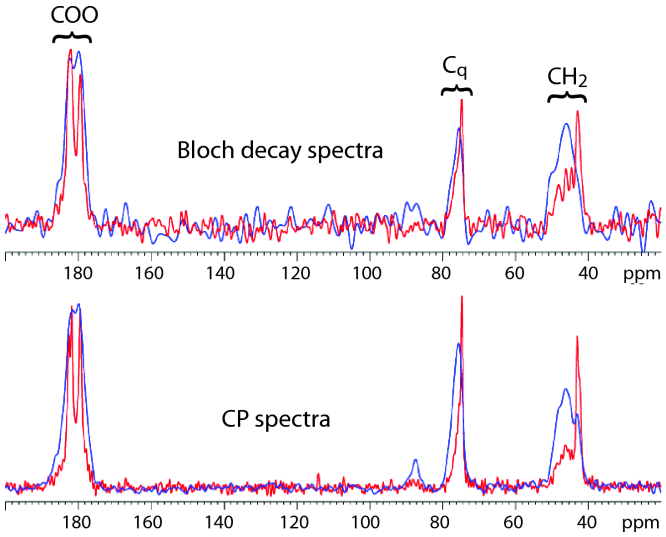

Fig. 6. **A:** The unit cell of the model the lowest energy structure for OCP-citrate (model **A**) fitting experimental ^{13}C NMR and PXRD data, with a composition of $Ca_{16}(PO_4)_8(HPO_4)_3(HCIT).10H_2O$; HCIT = $HOOC.CH_2.C(OH)(COO^-)CH_2COO^-$. Note that one of the CH_2-$CtOOH^-$ branches is 'dangling', *i.e.* extended out into the water channel and not coordinated to any of the calcium ions. **B:** Unit cell of a structure of the same composition that is 29 kJ mol^{-1} higher in energy than model **A** (model **B**), in which the whole citrate anion has been rotated ~180° with respect to the *b* axis, see Table S1 for details. **C:** Unit cell of a structure of the same atomic composition but chemical formula $Ca_{16}(PO_4)_8(HPO_4)_2(H_2PO_4)(CIT).10H_2O$ (model **C**) (83 kJ mol^{-1} higher in internal energy than model **A**, see Table S1 for further details).

non-crystallinity. This is precisely what makes it interesting from the point of view of a model of how citrate may be incorporated

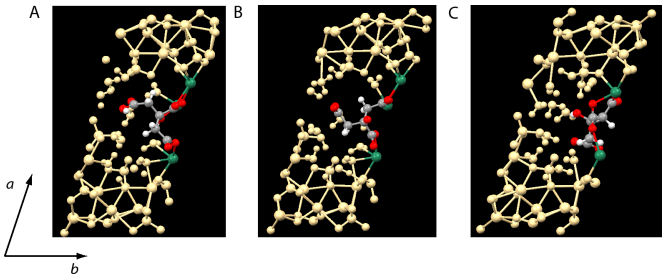

Fig. 7. Experimental PXRD diffractogram of OCP-citrate (red) and calculatedPXRD pattern (blue) corresponding to model **A** shown in Figure 7 (a), assuming a preferred crystal orientation of (100). Selected reflections are labelled; remaining signals are superpositions of several reflections. Inset: Calculated ^{31}P chemical shifts for the OCP-citrate structure shown in Figure 7 (a) marked with lines, relative to the experimental ^{31}P Bloch decay NMR spectrum.

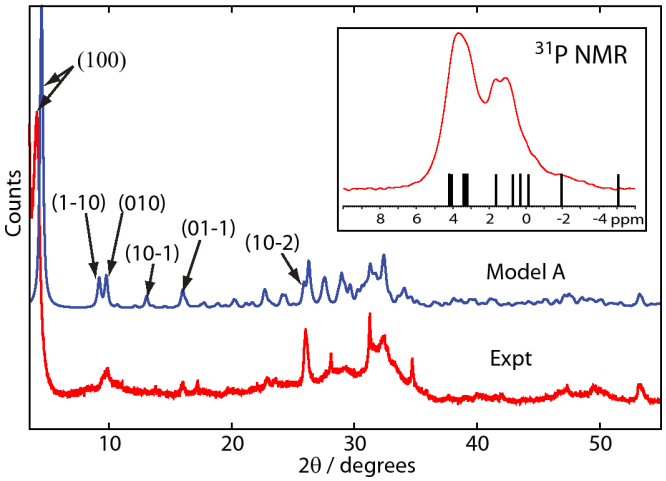

Fig. 8. $^{13}C\{^{31}P\}$ REDOR spectra of adult horse limb bone for the region of the spectrum where any citrate methylene and quaternary carbon signals are expected for the REDOR dephasing times indicated in the figure. The black spectrum in each case is the reference spectrum and the red spectrum, the REDOR spectrum. Signals reduced in intensity (dephased) in the REDOR spectrum with respect to the reference spectrum are due to ^{13}C carbons close in space to phosphorus, i.e. bone mineral. Those spectral regions that suffer significant dephasing that are referred to in the text are indicated.

into bone mineral, because as described in the introduction, a degree of disorder in the atomic level structure of bone mineral is necessary both in order to minimise impact of forming bone mineral on the surrounding organic matrix in bone and for the desirable mechanical properties of bone as a material. Thus, OCP-citrate is a potential model for the incorporation of citrate in bone mineral. In order to explore this potential, we first need to develop a structural model for the OCP-citrate double salt which naturally takes account of its structural disorder. Then we examine what evidence there is for such a phase in bone mineral and finally, what implications the structure (and dynamics) of such a phase has for the biological and mechanical properties of bone.

Results and Discussion

In order to develop a quantitative structure for OCP-citrate, we began from the OCP structure, since all previous work and our own shows that the OCP-citrate structure is strongly related to that of OCP. Multinuclear solid-state NMR spectroscopy was used to glean information about the environment of the phosphatic and citrate anions in the structure. We used this information to build a series of possible structural models which were then

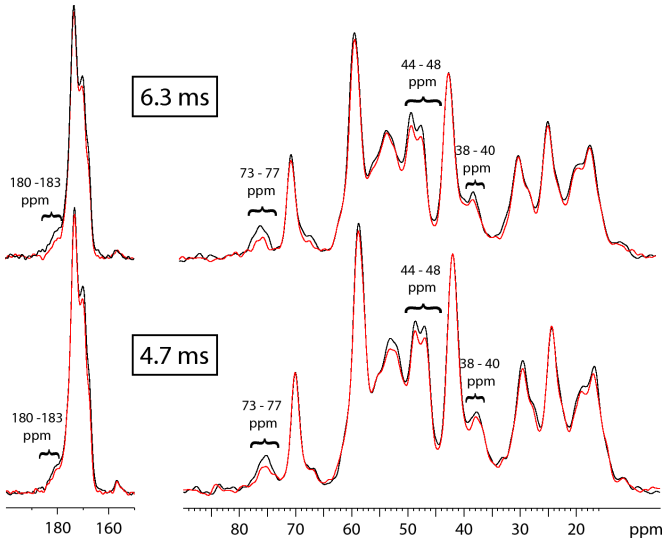

Fig. 9. Comparison of the ^{31}P NMR spectrum of bone (red) and that of the proposed model of bone mineral (black) which consists of a supercell structure comprised of three unit cells of hydroxyapatite, two of OCP and one of OCP-citrate, formed by summing the experimental ^{31}P NMR spectra for pure hydroxyapatite (dark blue), OCP (light blue) and OCP-citrate (green) in the total intensity ratio 3:2:1. The experimental spectra of hydroxyapatite and OCP have 200 Hz of Gaussian linebroadening applied to simulate disorder in the model structure.

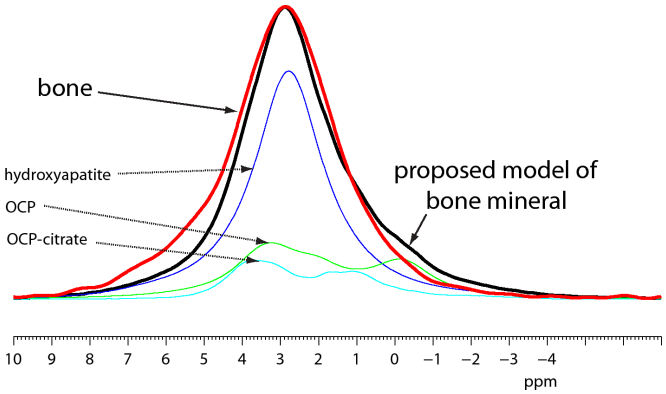

Fig. 10. ^{17}O DFS NMR spectra of (fresh) sheep bone (blue), OCP-citrate (red; 5% ^{17}O-enriched in the phosphate oxygens only), 5 % ^{17}O -enriched hydroxyapatite (green) and bone mineral soaked in aqueous citric acid (cyan). The individual spectra have been scaled so that the magnitude of the apatitic orthophosphate peak (truncated in the figure) is equal to that from bone, in order to compare the relative non-apatitic phosphate populations. The oxygen site giving rise to each signal is highlighted in red. The signals below 0 ppm are due to water, those above 150 ppm due to organic compounds (the organic matrix in the bone samples and citrate in OCP-citrate and the bone soaked in aqueous citrate), as indicated.

geometry-optimized using first-principles electronic structure calculations via CASTEP (19–21). The calculated NMR parameters and powder XRD patterns for the resulting optimized structures compared with experimental data, in order to determine the plausibility of each structure, which we defined as the degree to which the NMR parameters and powder XRD pattern calculated for a model structure agrees with the experimental data. The "true" structure, because of its inherent disorder, is best described as the coexistence of a set of structures in this approach and our ultimate goal here is to find a set of structures that defines the range of structural disorder within OCP-citrate and to determine if there is any dynamical interchange between the structures.

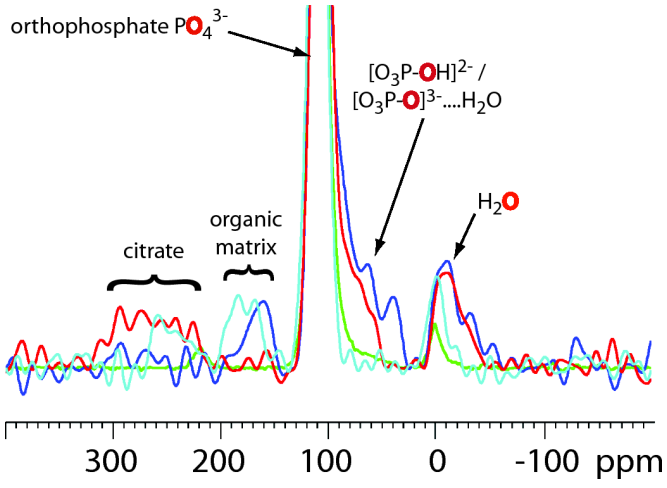

Fig. 11. ^{17}O DFS NMR spectra of (fresh) sheep bone (blue), OCP-citrate (red; 5% ^{17}O-enriched in the phosphate oxygens only), 5 % ^{17}O -enriched hydroxyapatite (green) and bone mineral soaked in aqueous citric acid (cyan). The individual spectra have been scaled so that the magnitude of the apatitic orthophosphate peak (truncated in the figure) is equal to that from bone, in order to compare the relative non-apatitic phosphate populations. The oxygen site giving rise to each signal is highlighted in red. The signals below 0 ppm are due to water, those above 150 ppm due to organic compounds (the organic matrix in the bone samples and citrate in OCP-citrate and the bone soaked in aqueous citrate), as indicated.

Thus, we begin our discussion here with an analysis of the NMR and powder XRD structural characterization of OCP-citrate that we used to derive possible structural models for geometry optimization.

Characterization of OCP-citrate

OCP-citrate was synthesised and its identity confirmed as described in the Supplementary Information - text, with the synthesis being performed six times to ensure a consistent product was obtained. Microanalysis of our OCP-citrate samples (see SI for details) gave a carbon content of 3.49 ± 0.16 wt%, Ca/P ratio of 2.01 ± 0.55 and a compositional formula of $Ca_{16}(PO_4)_8(HPO_4)_3$ (HCIT).(11± 1)H_2O, all in agreement with the stoichiometric approximation to the structural formula (14, 22), in particular, the idea that there is one citrate anion per unit cell.

SEM and TEM (Fig S1) shows that OCP-citrate crystallizes into well-formed crystals of constant morphology, typical dimensions being 790±100 nm × 100±30 nm × ~20-50 nm. The powder XRD pattern for freshly-synthesised OCP-citrate is shown in Figure 2; as found in previous work (14, 18), there is a significant shift in the scattering angle associated with the (100) reflection upon inclusion of citrate: 4.85° in OCP compared with 4.09° in OCP-citrate, indicating the expansion of the OCP unit cell along the *a*-axis to accommodate the citrate anions (d_{100} = 2.16 nm for OCP-citrate; d_{100} = 1.969 nm for OCP) in the (100) plane of the unit cell structure. Otherwise, the powder XRD pattern of OCP-citrate is similar to that of OCP, although the majority of the reflections are significantly broadened compared to those for OCP, as also found in previous work (14), indicating a material containing some element of atomic-level disorder. That some reflections remain sharp indicates a preferred orientation for the OCP-citrate crystals. Such a situation was found previously for OCP-succinate (18) where it was determined that the large flat face of those crystals corresponded to the (100) plane. That there is restricted growth of the crystals in the [100] direction would be consistent with disorder in the (100) plane, leading to imperfect stacking of unit cells along this direction. SAED on individual crystals (Fig S1) similarly indicates atomic position disorder within the crystals.

Characterizing the atomic structural disorder is of course a key requirement in this work and requires a characterization technique that relies on local structure, rather than long range order as diffraction methods do. Solid-state NMR spectroscopy is an ideal technique from this point of view, and it is to this that we turned, both to characterize the nature of the atomic disorder in OCP-citrate and to glean information on the position of the citrate anion in the OCP-citrate structure. Solid-state NMR spectroscopy has previously been used to gain atomic-level insights into the structure of OCP-succinate (23), but there have been no reports of solid-state NMR spectra of OCP-citrate. The spectra presented in this section are therefore shown, where appropriate, with comparable spectra of OCP.

The ^{1}H NMR spectrum of OCP-citrate (Fig S2), is dominated by a broad signal centred at ~5.5. ppm due to the water in the structure (24), and (presumably) overlies signals from citrate ^{1}H as well. The water ^{1}H signal in OCP is motionally narrowed, due to the mobility of the water molecules in that structure (24–26). The 5.5 ppm signal due to water in OCP-citrate is significantly broader than the water ^{1}H signal of OCP (Fig S2), indicating that the water molecules in OCP-citrate are reorienting more slowly or through a smaller amplitude or both compared to OCP. This suggests that the inclusion of citrate within the structure is interfering with the water channel which lies along the crystallographic *c*-axis in the so-called hydrated layer of OCP (Fig 1). This is consistent with the citrate anion replacing one of the hydrogen phosphate ions which line the water channels (11, 14) with the citrate anion protruding into the water channel.

The environment and structure of the citrate anion in OCP-citrate are both readily probed via ^{13}C Bloch decay (BD) and cross-polarization (CP) NMR spectra of the material (Figure 3). The carboxylate carbons give three signals, two well resolved at 179.5 and 182 ppm (labelled COO(**1**)) and COO(**2**) respectively, see Fig 3) and a shoulder at ~183 ppm (labelled COO(**3**)). The quaternary carbon (C_q) gives a signal whose maximum intensity is at 75 ppm, with a broader tail of shoulders to high frequency, whilst the methylene carbons give two signals, a sharper one centred at 43 ppm (labelled CH_2(**1**)) and a broader one centred at 46 ppm (CH_2(**2**)). Analysis of the integrated intensities in the Bloch decay ^{13}C NMR spectrum gives the ratio of COO : Cq : CH_2 signal intensities as $\sim 3:1:2$, as expected given the chemical formula of citrate ($C(OH)(COO^-)(CH_2COO^-)_2$). Deconvolution of the three carboxylate signals shows that they have close to equal intensity within the limits of error so they can be assigned to the three carboxylate groups of a single citrate environment. The signals are however broader than one would expect for a highly ordered environment (the ^{13}C spectrum of crystalline calcium citrate is shown in Fig 3 as an example of linewidths expected for highly ordered environments); thus it seems likely there is some disorder or heterogeneity in these three carboxylate environments.

The two methylene signals, CH_2(**1**) and CH_2(**2**), also have equal intensities and so can be assigned to the two methylene carbons of a single citrate environment as for the carboxylate signals. Clearly then, the two methylene groups of the single citrate environment in the structure are inequivalent, not surprising, given that the OCP unit cell and the citrate anion have incompatible symmetries: the OCP unit cell structure lacks any symmetry except a centre of symmetry, and citrate is not centrosymmetric. More importantly, the methylene group that gives rise to the broad ^{13}C signal (again, comparing with the linewidths for crystalline calcium citrate in Fig 3) must be disordered in some way as it gives rise to a distribution of ^{13}C chemical shifts. So at least one source of disorder in the OCP-citrate material is associated with one of the citrate methylene groups.

The most likely source of the disorder affecting a methylene group in citrate is conformational. Multiple conformations for one of the $CH_2COO(H)$ branches of the citrate anion, i.e. multiple torsional angles about the $C_q - CH_2$ bond, would give rise to a different ^{13}C chemical shift for the methylene carbon for each conformation, a consequence of the so-called γ-gauche effect. Multiple conformations of one of the $CH_2COO(H)$ branches would also be expected to give a chemical shift distribution for the quaternary carbon via the same effect, which is indeed observed: the tail of shoulders to the high frequency side of the main resonance (Fig 3). Likewise, one would expect some ^{13}C chemical shift distribution for the terminal COO(H) in the disordered $CH_2COO(H)$ branch; there is a broad tail of intensity on the low frequency side of the lowest frequency carboxylate signal (COO(**1**), 179.5 ppm) and so we tentatively assign this resonance to the terminal carbon of the disordered $CH_2COO(H)$ branch of the citrate anion.

The conformational disorder of the CH_2(**2**)COO(H) branch may be static or dynamic. We investigated the possibility of dynamic disorder by cooling a sample of OCP-citrate to 200 K and re-recording ^{13}C CP MAS spectra. Cooling the sample to 200 K does not change the relative intensities of the CH_2(**1**) and CH_2(**2**) signals, which remain 1:1, but it significantly increases the resolution in the ^{13}C spectrum (Fig 4), with the broad CH_2(**2**) signal (46 ppm) beginning to resolve into sharper components. This observation is consistent with the citrate CH_2(**2**)COO(H) branch undergoing reorientational motion at room temperature and that motion being slowed by lowering the temperature so that signals from individual conformers are beginning to be resolved at the lower temperature. The resolution of the sharper CH_2(**1**) methylene signal also increases at 200 K, with a shoulder resolving on its low frequency side, suggesting that this methylene group too has more than one possible conformation or orientation.

Lowering the temperature to 200 K[1] also markedly increases the cross-polarisation efficiency the broad, CH_2(**2**) (46 ppm) methylene signal (Figure 4), the high frequency tail of the quaternary carbon signal (75 ppm) and the low frequency tail of the COO(**1**) carboxylate signal (179.5 ppm) relative to the other signals in their respective spectral regions. This is consistent with there being room temperature molecular motions affecting the CH_2(**2**) methylene, COO(**1**) carboxylate and the quaternary carbon environments giving rise to the high frequency tail above 75 ppm, reducing cross polarization efficiency at room temperature by averaging the ^{1}H-^{13}C dipolar coupling which mediates it. Thus, it would appear that the disorder of the citrate CH_2(**2**)COO branch is dynamic at room temperature (and still to some extent at 200 K). That the CH_2(**2**)COO branch is able to reorient dynamically strongly suggests that it is not coordinated to calcium (or any other species), but is relatively free to rotate. Since the citrate anion is contained in the hydrated layer of the OCP structure (see Fig 1), the most likely orientation of the CH_2(**2**)COO branch which permits relatively facile reorientation is for it to be protruding into the water layer itself. This feature will be used when constructing possible models of the OCP-citrate unit cell structure for subsequent geometry optimization.

The nature of the phosphate sites in OCP-citrate and how their environment differs from those in the parent OCP compound are readily assessed by ^{31}P NMR. The ^{31}P NMR Bloch decay spectrum of OCP-citrate (Figure 5) shows significantly broader lines than the corresponding spectrum for the parent OCP compound (also shown in Fig 5 for comparison). Some

[1] Lowering the temperature below 200 K led to the formation of ice crystals on the sample suggestive of water loss from the sample, and thus possible transformations of the crystal structure.

reduction in the resolution of the ^{31}P NMR spectrum is expected because of the lack of symmetry within the crystallographic unit cell once citrate is incorporated - it is impossible to substitute citrate into any of the phosphate sites of OCP without violating the centrosymmetric condition of the OCP unit cell as citrate itself does not contain a centre of symmetry. As a result, instead of twelve pair-wise equivalent ^{31}P environments giving rise to a total of five distinct ^{31}P signals as in OCP, the OCP-citrate system has eleven distinct ^{31}P environments within the unit cell. Nevertheless, in a highly crystalline compound, one would still expect to resolve some of the eleven expected signals or observe them as shoulders on other signals, but such resolution is lacking indicating some disorder of the phosphate sites. Some structural disorder of phosphate sites close to the citrate anion is likely to be imposed by the conformational disorder of one $CH_2COO(H)$ branch of the citrate; the ^{31}P chemical shift is known to correlate strongly with P – O bond length (27) and is sensitive to O-P-O bond angle (28) so a small distribution in either or both of these arising from the presence of several different citrate conformations within a single crystal would be expected to give rise to a distribution of ^{31}P chemical shifts for phosphate sites in the vicinity of the citrate anion. In turn, a distribution of phosphate structures/ orientations close to the citrate anion will have a knock-on effect for the phosphate sites more remote from the citrate, leading to some degree of linebroadening for all ^{31}P signals. A further source of linebroadening in NMR spectra is inefficient ^{1}H decoupling arising from mobile ^{1}H; we will return to this point later.

Comparing the ^{31}P signal frequencies between OCP and OCP-citrate in Figure 5, there is a clear shift of the signals in the low frequency part of the spectrum, such that the P3, P5 and P6 signals of OCP appear to have been shifted to higher frequency in OCP-citrate (see Fig. 5 for signal assignment). As described in the introduction, the citrate anion is hypothesized to substitute for one of the P5 hydrogen phosphate sites in the OCP structure. As such, one might expect the presence of the citrate anion to perturb the ^{31}P signals from the nearby P3 (formally orthophosphate hydrogen bonded to water) and P6 (hydrogen phosphate) sites which neighbour, indeed are hydrogen bonded to, the P5 sites in the OCP structure. The low chemical shift of the P3, P5 and P6 ^{31}P signals for OCP (-0.1 ppm, P6; -0.3 ppm, P3, P5) (25) results from the hydrogen bonding network that extends between all six of these groups in the OCP structure and the water molecules between them. In the OCP-citrate compound, only a small broad signal remains in the spectral region below 0 ppm with two new, broad, overlapping signals at higher frequency (centred at 1.1 and 1.6 ppm) largely replacing the low frequency OCP signals. Thus we conclude that the incorporation of citrate anions into the OCP structure has for the most part destroyed the cooperative hydrogen bonding between the phosphatic sites of the hydrated layer that led to the low frequency signals for those groups in OCP.

The question remains as to the assignment of the ^{31}P signals at 1.1, 1.6 ppm in OCP-citrate. ^{1}H-^{31}P 2D heteronuclear correlation (HETCOR) spectra allow assignment of the ^{31}P signals by indicating which ^{1}H and ^{31}P sites are close in space and ^{1}H-^{31}P 2D HETCOR spectra for OCP-citrate (Fig S3) show that the overlapping signals 1.1, 1.6 ppm are correlated with both water and hydrogen phosphate ^{1}H signals at short mixing times (500μs), indicating that these signals are due (at least in part) to hydrogen phosphate sites. There may well be *orthophosphate sites* hydrogen bonded to water, i.e. P3 sites, giving signals in this same ^{31}P spectral region, but these are impossible to distinguish from the hydrogen phosphate signals as their correlation signals will overlap with those of the expected hydrogen phosphate ^{31}P - water ^{1}H correlation.

The apatitic orthophosphate sites (P1, P4 – see Fig 1) in OCP-citrate give the broad signal centred at 3.7 ppm (cf. 3.2 and 3.6 ppm in OCP for P1 and P4 respectively). The 2D ^{1}H-^{31}P HETCOR spectrum of OCP-citrate shows a correlation between the apatitic orthophosphate sites and water ^{1}H even at short mixing times, indicating that there is significant dipolar coupling between water ^{1}H and the ^{31}P nuclei associated with these sites. We note that given this, mobility of the water molecules dipolar coupled to the orthophosphate sites will affect the ^{1}H decoupling process for the ^{31}P signals from these sites, rendering the ^{1}H decoupling less effective and will undoubtedly contribute to the linebroadening of their signals.

Also of interest in the 2D ^{1}H-^{31}P HETCOR spectrum at long mixing times (10 ms, Fig S3) is that it shows an additional ^{1}H signal at 2.7 ppm, which we can assign to citrate methylene ^{1}H – this will be important when comparing NMR parameters calculated for trial OCP-citrate structures with experimental data later.

Water content of OCP-citrate

Previous studies of OCP-carboxylic acid double salts have found a wide variation in water content depending on the carboxylic acid involved (14, 16, 22). To some extent this is not surprising, as the water content will depend on the amount that the unit cell expands to incorporate the carboxylic acid anion. However, the water content is not entirely correlated with the degree of unit cell expansion and moreover, significantly different water contents were found for the OCP-citrate compound between samples in a previous study (14).

In our own work, we have observed mass loss during recording of NMR spectra and powder XRD, attributed to water loss and confirmed by ^{1}H NMR and FT-IR. Given that one of the citrate $CH_2COO(H)$ branches is likely to be protruding into the water layer (as discussed with reference to the ^{13}C NMR data), and therefore that the citrate conformation is likely to be at least to some extent interdependent on the water content, we undertook a more detailed study of the effect of changing the degree of hydration of the sample.

Fig S4 shows the powder XRD pattern from dehydrated OCP-citrate material in which the water loss of 6.6 % by weight corresponds to a loss of 7.6 water molecules per unit cell; the d_{100} reflection has clearly moved to higher 2θ, indicating a shrinking of the unit cell along the *a* axis with removal of water. In addition, some of the reflections have broadened indicating further disordering. The further disordering is borne out by SEM (Fig S5), ^{31}P NMR (Fig S6) and ^{1}H NMR (Fig S7) spectra. Figure 6 shows ^{13}C CP and BD spectra of the dehydrated material. There is a clear shift in the intensity distribution towards higher frequency for the CH_2 and quaternary carbon signals, and significant linebroadening, consistent with conformational disorder now affecting both methylene groups. These data will be used when assessing the possible involvement of an OCP-citrate like structure in bone mineral.

Constructing Structural Models of OCP-citrate

Our next step was to use the structural information gleaned from the NMR data discussed above, along with that from powder XRD and FT-IR (14), to construct possible models for the unit cell structure of OCP-citrate that we then geometry optimized.

Specifically, the structural information used in constructing possible unit cells structures was that:

• There is only sufficient carbon content for one citrate per unit cell.

• Citrate replaces a hydrogen phosphate site and so citrate was mainly included in the trial structures as a singly protonated,

2- anion, denoted $HCIT^{2-}$, to achieve charge balance (though 3-citrate anions were included in some models – see Table S1).

• The citrate is most likely to replace a P5 hydrogen phosphate anion (FT-IR data (14)), so one (or more) P5 hydrogen phosphate anions was removed from the OCP structure.

• The hydrogen phosphate sites are all in the hydrated layer of the OCP structure (Fig 1) and so the citrate anion was placed in the hydrated layer in all trial structures.

• Incorporation of citrate expands the unit cell along the *a* axis.

• The OCP-citrate chemical composition has been determined here to be close to $Ca_{16}(PO_4)_8(HPO_4)_3$ (HCIT).(11± 1)H_2O, although the water content is demonstrably variable.

• One CH_2(COO(H) branch of the citrate is conformationally disordered and is likely to be protruding, uncoordinated, into the water layer.

Ten possible models were geometry optimised using first principles electronic structure calculations as implemented in CASTEP (19, 29, 30), and the NMR parameters and powder XRD patterns associated with the resulting structures calculated; Table S1 in Supplementary Information details the eight geometry-optimized structures which give NMR parameters in some way comparable to experiment. The calculated ^{13}C NMR parameters (Table S1 and Table 1 below) were then used to determine if a structural model had a realistic environment for the citrate anions, whilst bearing in mind that the calculated values of ^{13}C shifts are those for 0 K, whereas experimental values are determined at room temperature. In addition, we took into account that the accuracy of the ^{13}C chemical shifts in these calculations is ∼1-2 % of the chemical shift range of ^{13}C, *i.e.* ± (2-4) ppm (31).

In evaluating the geometry-optimized models of OCP-citrate, a number of trends became apparent.

• NMR calculations on seven of our models showed a significant separation of the two ^{13}C NMR methylene signals (∼ 2 – 12 ppm difference in chemical shift, depending on the structural model) in agreement with ^{13}C NMR experiments.

• In general, the CASTEP calculations indicated that the ^{13}C COO^- signals at higher frequency are likely to correspond to Cq-COOH or Cq-COO^- environments rather than –CH_2COOH, consistent with reports of solution-state NMR of metal-citrate complexes (32, 33).

• In metal-citrate complexes, citrate can act as a tridentate ligand, coordinating to metal centres *via* the α-hydroxycarboxylate (*i.e.* Cq-OH and Cq-COO^-) and one of the terminal carbonyls ($CtOO^-$) . However, the structures that gave rise to ^{13}C chemical shifts closest to experiment for the dominant Cq ^{13}C signal (∼75 ppm) are those in which Cq-OH is *not* coordinated to calcium; structures in which Cq-OH is coordinated to calcium give unrealistically high ^{13}C chemical shifts for both Cq and Cq-COO^-. This suggests that such a binding mode is not preferred in OCP-citrate and so these structures were not considered further.

• In order to predict the effect of hydration level on the ^{13}C chemical shifts, the geometry of two of the models (Models **A** and **B** in Supplementary Information, Table S1) were reoptimised after inclusion of additional water molecules, and the NMR parameters recalculated. With a single exception, the ^{13}C chemical shift of all of the CH_2 and Cq environments moved to lower frequency on addition of water ($^{\triangle}\delta(CH_2) \sim$ -(3-5) ppm, $^{\triangle}\delta$(Cq) ∼ -(1-2) ppm), and the ^{13}C chemical shifts of the ^{13}Cq-COO^- and $^{13}COO_t$ sites moved to higher frequency ($^{\triangle}\delta$(Cq-COO) ∼ +(2-5) ppm, $^{\triangle}\delta(COO_t) \sim$ +(1-3) ppm), consistent with the experimental ^{13}C NMR spectrum of the dehydrated compared with the hydrated material.

• Structures in which one or more of the structural criteria outlined previously were ignored did not give pXRD and NMR data consistent with experiment.

The lowest energy structure (structure **A** in the discussion that follows) which fits experimental ^{13}C, ^{1}H and ^{31}P NMR and powder XRD data, and which is in accord with the expected composition is shown in Fig. 7 (a). The citrate anion in this structure has one CH_2-$COOH^-_t$ branch "dangling" in the water channel of the OCP-citrate structure, not coordinated to calcium ions, but surrounded by water. This CH_2-$COOH_t$ branch is primarily constrained only by the presence of the (mobile) water molecules and thus can be expected to have a distribution of rotational conformers at room temperature, giving disorder in the unit cell structure and a distribution of chemical shifts for the associated ^{13}C methylene carbon signal and for the quaternary carbon signal, as observed experimentally. The terminal carboxylate group of this dangling branch is not coordinated to any calcium ions, and thus its chemical shift would not be expected to be very strongly affected by the orientation of the branch, which again, is as observed experimentally.

The calculated and experimental ^{13}C chemical shifts for this structural model are compared in Table 1. Agreement between experimental and calculated chemical shifts is good, especially when one takes into account the fact that the ^{13}C chemical shifts are calculated for a single 0 K structure whilst experimental measurement is made at room temperature where there is a distribution of citrate conformers. In particular, the lowest frequency carboxylate ^{13}C chemical shift calculated, 178.6 ppm, corresponds to the (protonated) carboxylate group of the dangling, uncoordinated CH_2COOH branch of the citrate and the highest frequency methylene signal calculated, 45.6 ppm, the methylene group of that same branch in structure **A**, both features as assigned previously on the basis of experimental observations.

Table 1: Comparison of the experimental ^{13}C chemical shifts for OCP-citrate and those calculated for structure **A.** For the experimental data, the observed ranges of chemical shifts are given for the broader signals. All values are given in ppm. The calculated chemical shifts for COOH(**1**) and CH_2(**2**) correspond to the uncoordinated CH_2COOH branch of the citrate anion in structure **A**.

	COOH(**1**)	COO(**2**)	COO(**3**)	C_q	CH_2(**1**)	CH_2(**2**)
Experimental	179.5	182	183	75 - 77	42 - 44	44 - 49
Calculated	178.6	181.7	184.7	79.8	37.8	45.6

Comparison of the powder XRD pattern for the **A** structural model, assuming a (100) preferred orientation as initially predicted, is shown in Figure 8 and agrees well with the experimental pattern except that the (100) reflection in the calculated pattern appears at higher 2θ than in the experimental pattern, i.e. the *a* unit cell parameter is smaller in the **A** structural model than the experimental structure. This discrepancy is to be expected as model **A** is a structure calculated at 0 K, whereas the experimental XRD measurement is at room temperature and we would expect some unit cell expansion between 0 K and room temperature. There are some other discrepancies, but these are small, especially in view of the uncoordinated CH_2COOH branch of the citrate anion being conformationally disordered at room temperature, and each of those conformations is likely to be associated with a different spatial distribution of water molecules – in other words, the room temperature structure is in fact a dynamic combination of multiple structures.

Interestingly, a second structure **B** (Fig 7(b)) with the same chemical composition as **A** and with only a slightly less favourable internal energy (by 29 kJ mol^{-1}) in which the citrate anion is flipped ∼180° with respect to the *b* axis relative to structure **A** also

yields calculated ^{13}C chemical shifts consistent with experiment. Thus, the OCP-citrate structure may be further disordered by virtue of the orientation of the entire citrate anion; this feature would certainly explain the two signals that the CH_2(**1**) ^{13}C NMR signal begins to resolve into at 200 K, for instance. A third structure **C** (Fig 7(c)), 83 kJ mol^{-1} higher in energy than **A**, with the same atomic composition but with the chemical formula, $Ca_{16}(PO_4)_8(HPO_4)_2(H_2PO_4)(CIT).10H_2O$, gives ^{13}C NMR chemical shifts for the citrate anion that are consistent with those observed experimentally for partially dehydrated OCP-citrate. Structure **C** is a much more compressed structure; the hydrated layer is partially collapsed so that the citrate anion is wedged between the apatitic layers. This sort of structural collapse is a plausible model for a structure undergoing removal of water from the hydrated layer and is likely to be typical of the citrate environment found in the dehydrated material.

Evidence for an octacalcium phosphate citrate-like phase in bone mineral

The association of citrate with the mineral component of bone was previously demonstrated with NMR via a $^{13}C\{^{31}P\}$ REDOR experiment. This experiment identifies the carbon species in close spatial proximity to phosphorus, and as the very vast majority of phosphorus in bone is in the mineral component, the experiment effectively identifies the organic species in closest proximity to the mineral.

Figure 9 shows the $^{13}C\{^{31}P\}$ REDOR behaviour of adult horse limb bone. In each case, the pairs of spectra consist of a reference ^{13}C spectrum (black) and a REDOR dephased spectrum (red) in which signals due to ^{13}C sites close in space to ^{31}P are dephased, i.e. reduced in intensity, enabling the identification of the organic moieties close to bone mineral. For the bone sample, there is, as observed previously by us and others (34–36), clear dephasing in the 180 – 183 ppm, 73 – 77 ppm and 44 – 48 ppm regions (Fig 9) of the spectrum,[2] which corresponds closely to the signal frequencies for the citrate moiety in OCP-citrate, in particular those calculated for structure **C**, in which citrate anions are in compressed water layers, bridging between apatitc layers. In structure **C**, all the carbons in the citrate anion are between 0.36 and 0.46 nm from phosphorus atoms, which is consistent with the $^{13}C\{^{31}P\}$ REDOR dephasing behaviour observed for citrate in bone (2). It should be noted that bone subjected to REDOR experiments is inevitably partially dehydrated because of the effects of rf heating over the long period of time for which the NMR experiment runs and the nature of the sample preparation (37). Structure **A** predicts methylene ^{13}C NMR signals at 38 and 46 ppm (at 0 K), structure **B** at 40 and 46 ppm and the REDOR spectra in Fig 9 also show dephasing in the 38 – 40 ppm region, as well as 44 – 48 ppm. Overall, the NMR data supports the existence of OCP-citrate like structures with varying degrees of hydration in bone mineral.

How could an OCP-citrate structure be incorporated into bone mineral? Bone mineral has a significant component with a structure related to hydroxyapatite of course (albeit with many substitutions). It is well known that hydroxyapatite and OCP can form an epitaxial interface with the minimum of interfacial energy (38, 39) between the (200) plane of hydroxyapatite and the (100) plane of OCP. Hydroxyapatite layers could be incorporated into the apatitic layers of OCP-citrate in a similar manner. The thickness of bone mineral platelets has been estimated to be ~2.5 nm (40); this measurement via NMR effectively estimates the thickness of mineral between mobile water layers. The thickness of the mineral layer in OCP-citrate between its mobile water layers is 1.2 – 1.4 nm. Thus adding one unit cell of hydroxyapatite to the (100) plane of OCP-citrate, i.e. intersecting the OCP-citrate structure with a unit cell of hydroxyapatite, which has a thickness of 0.91 nm along its *a* dimension, would create a supercell with a mineral layer thickness similar to that in bone of ~ 2.2 nm.

If we take such a supercell as a model of at least a component of bone mineral, how much of such a structure might be present in bone mineral overall? The citrate content of bone is estimated at between 1 – 2 % by weight, whilst the mineral component is 60 – 70 % by weight. If we assume that all the citrate in bone is associated with the bone mineral, then the citrate comprises of order 1.5 – 3 % of the mineral by weight. Citrate in OCP-citrate constitutes 6.2 % of the weight of the hydroxyapatite-OCP-citrate super-unit cell formed by adding one unit cell of hydroxyapatite to the (100) plane of OCP-citrate; thus if we take the supercell structure as a model of bone mineral, 1/2 to 1/4 of the supercells would contain citrate. The absence of citrate in the remaining supercells could be modelled by replacing the OCP-citrate component with simply OCP, but with an expanded unit cell along the *a* direction for the OCP component relative to pure OCP, to match the neighbouring OCP-citrate unit cells. Thus the atomic positions within the OCP components of the supercells would presumably be disordered to some extent as a result of the expansion of the OCP component. Thus the presence of citrate introduces a further atomic disorder; in addition, the random presence of citrate in some supercells and not in others is a yet further source of disorder.

Such a structure for bone mineral naturally explains a number of significant observations. Several studies have shown that bone mineral has strongly bound water associated with it (4, 5, 41–43), with water ^1H of order ~2.3 – 2.55 Å from mineral ^{31}P (43). The water has previously been assumed to be bound to the surface of mineral platelets, but the HA-OCP-citrate supercell model suggests an alternative explanation, where the water is effectively trapped inside the mineral structure, which would account for its very strong binding and proximity to mineral phosphate. If water is on the surface of mineral particles, its difficulty of removal is not straightforward to explain. Moreover, if we think of the water layer in the HA-OCP-citrate structure as being between two mineral apatitic "surfaces", those "surfaces" are naturally lined with HPO_4^{2-} which previous studies have identified as being the predominant surface species in hydroxyapatite (44) and bone mineral (5) particles. Interestingly, other NMR work suggests that the protons associated with hydrogen phosphates in otherwise apatitic compounds are mobile (45) Early studies of bone mineral struggled to detect any hydroxyl groups, characteristic of the hydroxyapatite structure. When hydroxyl groups were eventually detected (by NMR), they were found to be present at only ~20 % of the concentration expected for hydroxyapatite(4). It is difficult to see how bone mineral could be composed of a largely apatitic structure given this fact. However, a structure comprised of HA-OCP-citrate allows straightforward explanation. Figure 10 shows what the ^{31}P NMR spectrum of the proposed HA-OCP-citrate material might look like, based on experimental ^{31}P NMR spectra for its pure components, i.e. hydroxyapatite, OCP-citrate and (disordered) OCP (modelled by a linebroadened spectrum of OCP) in a ratio of 3:1:2, i.e. 1/3 of the supercells containing citrate. Of course the calculated ^{31}P NMR spectrum does not exactly replicate that of bone and nor can it be expected to: bone mineral is known to contain many ionic substitutions, in particular carbonate, which affect the ^{31}P NMR spectrum (46) and the interface regions between the hydroxyapatite, OCP and OCP-citrate unit cells will have modified structures from the pure com-

[2] The other signals which show (small) dephasing can all be assigned to lysine and hydroxylysine, which in bone collagen are glycosylated with galactosyl and glucosyl galactosyl. These sugar species also contribute to the signal in the 74 – 77 ppm region of the spectrum and presumably account for the stronger dephasing of this signal than the signal assigned to citrate methylene carbons.

pounds and thus different ^{31}P chemical shift distributions from the pure compounds used to produce a hypothetical ^{31}P NMR spectrum for our proposed bone mineral model. Nevertheless, the hypothetical spectrum in Fig. 10 has a closely similar chemical shift distribution to that of bone mineral.

Furthermore, we have noted that the disordering of the unit cell structure imposed by the presence of the citrate anions in the OCP-citrate structure limits the growth of OCP-citrate crystals along the *a* axis and results in flat, platelet morphology for the crystals. A similar mechanism would readily account for the similar morphology of bone mineral particles.

Finally, there is abundant atomic species in bone mineral that, to the best of our knowledge, has yet to be employed in the study of bone mineral structure, namely oxygen. ^{17}O is the only NMR-active isotope of oxygen; it is a quadrupolar nucleus (I = 7/2) with low natural abundance, but its NMR spectra are accessible at high field. ^{17}O NMR is a potentially valuable tool, as the mineral phosphate oxygens are likely to be highly sensitive reporters of the phosphatic environment. To this end, Figure 11 compares ^{17}O double-frequency sweep (DFS) NMR spectra for bone with those of (5 % ^{17}O-enriched) hydroxyapatite, bone mineral soaked in citric acid and OCP-citrate. Apatitic orthophosphate signals are expected in the 90 – 120 ppm range, whilst hydrogen phosphate OH ^{17}O will be much lower, around 60 – 90 ppm, and hydrated orthophosphate somewhere between these two regions. It is clear that neither hydroxypapatite nor citrated bone mineral give spectra comparable to bone in this crucial region of the spectrum, crucial because it is the presence of acidic and hydrated phosphate groups in bone mineral that distinguish it from pure hydroxyapatite mineral. However, OCP-citrate provides a reasonable match to the bone ^{17}O NMR spectrum.

Conclusions

The incorporation of citrate ions into the crystalline structure of bone mineral can account for many well known structural features of bone mineral, such as the very small thickness of mineral crystals, the strongly bound water, previously assumed to be associated with mineral crystal surfaces and the presence of significant quantities of hydrogen phosphate ions, in addition to the expected orthophosphate of pure hydroxyapatite.

The structural model of the citrate incorporation into the crystalline lattice of bone mineral proposed here suggests a role for citrate not previously encountered – that it acts to disorder the atomic structure of bone mineral. We further hypothesise that such a disordering role is of fundamental importance in biomineralization. The ordering of mineral ions into a crystalline lattice is always accompanied by a decrease in entropy for those mineral ions. The second law of thermodynamics says that the entropy of the Universe can only *in crease*. Thus a decrease in entropy must be compensated by an increase in entropy elsewhere in the system, the system in this context being all that is in thermal contact with the mineral. In a calcified tissue like bone, what is in thermal contact with the mineral particles is the surrounding organic matrix and water. Thus it is these components that must suffer an in crease in entropy, that is become more disordered, upon crystalline mineral formation. Free water molecules released from ions during crystallization have substantial disorder associated with them. However, water molecules released from ions during biomineralization within an organic matrix are not free. They are bound to mineral crystal surfaces and restricted to spaces with nanoscopic dimensions within the organic matrix where they further associate with protein molecules (including proteoglycans where the sugar components bind significant numbers of water molecules). Thus a large decrease in entropy of mineral ions because of formation of well-ordered mineral crystals is likely to necessitate at least some disordering of the surrounding organic matrix.

It has previously been proposed that citrate ions are coordinated to surfaces on the exterior of bone mineral particles (1) via all three of their carboxylate groups, as the available NMR data showed that all three carboxylate groups are in close proximity to phosphate. However, in this scenario, the citrate anion conformation would be significantly restricted, reducing the entropy of the organic matrix-mineral system in bone whose entropy has already been reduced by the ordering of mineral ions into crystalline platelets. This would mean a large compensating entropy change towards disorder would be needed in the surrounding organic matrix and water upon matrix calcification. But in a biological system, disordering a matrix organised for cell and ligand recognition is an uncontrolled and therefore potentially dangerous process. In our proposed model of bone mineral, citrate anions bridge between apatitic mineral layers allowing the citrate to adopt a variety of conformations and orientations. In the model, the citrate anions are in hydrated layers of the mineral structure and different citrate orientations/ conformations are associated with different arrangements of water molecules to accommodate the citrate. We have shown that there are several different citrate orientations and likely many different citrate conformations that have similar energy and so are accessible at biological temperatures. Moreover, ^{1}H NMR shows that the water molecules surrounding the citrate anions are reorienting approximately isotropically on a ∼ms timescale and so also have a large number of different orientations accessible to them. Thus our proposed model for the structure of bone mineral would provide a much-needed source of disorder in the mineral phase, and so limit the compensating disorder that must occur in the organic matrix.

In this model, the presence of citrate is the key factor controlling the crystallinity of bone mineral, as its presence prevents the long range ordering that would be present in a pure hydroxyapatite structure, for instance, and its concentration controls the degree of order that can be obtained in the hydrated, citrated layers between the apatitic layers. This feature could become important in explaining the changes to bone mineral crystallinity in metabolic diseases (8) and understanding the mechanical properties of bone at a molecular level. Furthermore, the disordering imposed by the presence of citrate anions in the mineral structure naturally restricts growth of the mineral crystals in the [100] direction and so may explain the flat platelet morphology of bone mineral particles.

Materials and Methods

Synthesis: OCP-citrate was prepared using a previously published synthetic procedure (22) starting from α-tricalcium phosphate ($Ca_3(PO_4)_2$; α-TCP) prepared for us by the research group of Prof Serena Best, University of Cambridge using a standard procedure (47). All other reagents throughout the work were purchased from Sigma-Aldrich except where explicitly stated otherwise and used without further purification. Full details (including synthesis of OCP are given in the Supplementary Information – text.

OCP-citrate (dehydrated): OCP-citrate (152 mg, 0.07 mmol) was stored over P_2O_5 under vacuum for 2 days (final mass 142 mg), and subsequently characterised by PXRD and solid-state NMR spectroscopy. The 6.6 % weight loss corresponds to a loss of 7.6 water molecules per unit cell.

Synthesis of ^{17}O-enriched OCP and OCP-citrate used ^{17}O-enriched orthophosphate (to prepare ^{17}O-enriched brushite in the former case and ^{17}O-enriched α-TCP in the latter case). 20 % ^{17}O-enriched orthophosphate solution was prepared as follows: ^{17}O-enriched H2O (1 g, 20 atom %, Cambridge Isotope Laboratories, USA) was added dropwise to P4O10 (2.70 g, ∼9.5 mM), followed by 150 mL of distilled water to quench the remaining P4O10. The solution was then acidified using0.1 M HCl and refluxed for ca. 1 week (additional HCl added daily). The product, a solution of ^{17}O-enriched H3PO4 (∼0.25 M), was free from poly-phosphate contamination as shown by solution-state ^{31}P NMR spectroscopy, and negative-ion electrospray ionisation (ESI) mass spectrometry indicated the enrichment level to be ∼10 % H3P(^{17}O)^{16}O3 and ∼10 % H3P(^{17}O2)^{16}O2.

Bone Samples

Sheep Bone: Distal sesamoid (heel) bone was taken from an adult sheep (more than one year old).

Adult Horse Bone: Horse limb cortical bone was taken from an adult horse used for general purpose exercise that was euthanised for humanitarian reasons unconnected with this work.

All bone samples were cryomilled before being packed into NMR rotors. Prior to cryomilling, samples were stored at -80ºC.

DFT Calculations

Working models of the OCP-CIT structure were created using the PyMOL Molecular Graphics System, version 1.3 Schrödinger, LLC. These models were then geometry optimised using CASTEP version 5.502 (conditions as per optimisation of OCP).

When determining ^{31}P chemical shifts from the chemical shieldings according to $\delta_{iso} \approx \sigma_{ref}-\sigma_{iso}$, with σ_{ref} = 275.3 ppm. In the case of ^{13}C chemical shifts, the calculated shieldings were plotted against experimental shifts, and the reference shielding set to the intercept of the line of best fit, where the gradient of the line was set to -1. Finally, the ^{1}H chemical shifts were calculated from the chemical shieldings using σ_{ref} = 30.18 ppm, which was used effectively in a recent study by Webber *et al.* (2).

The calculations were performed using the Darwin Supercomputer of the University of Cambridge High Performance Computing Service (http://www.hpc.cam.ac.uk/), provided by Dell Inc. using Strategic Research Infrastructure Funding from the Higher Education Funding Council for England.

Physical characterization

FTIR-ATR spectra were acquired using a PerkinElmer Spectrum One FTIR spectrometer with Universal ATR sampling accessory over the range 650-4000 cm^{-1} (resolution 4 cm^{-1}).

PXRD measurements were performed on a Philips X'Pert Pro powder diffractometer equipped with an X'celerator RTMS detector and using Ni-filtered CuKα radiation. Powder samples were mounted on at glass plates and data collection was performed over the range 2θ = 3 to 80º.

To prepare samples for TEM, a small amount of material was suspended in pure ethanol, and a drop of the suspension was applied to a holey carbon film grid and allowed to dry. Bright-field TEM was performed in a FEI Tecnai G2 electron microscope run at 200∼kV. Selected-area electron diffraction images were acquired using the same microscope at 200∼kV (spot size 7).

NMR Measurements

Solution-state ^{31}P NMR spectra of the ^{17}O-enriched orthophosphate solution were acquired using a Bruker 400 MHz Avance III spectrometer, equipped with a QNP Cryoprobe, at a ^{31}P frequency of 161.98 MHz and ^{1}H frequency of 400.12 MHz. The standard Bruker-supplied "zgpg30" pulse program was used (^{31}P π/2 pulse length 8.63 µs, WALTZ-16 decoupling during signal acquisition at ^{1}H field strength 3.13 kHz).

All solid-state ^{1}H, ^{31}P and ^{13}C NMR measurements were performed on a Bruker 400 MHz Avance spectrometer, equipped with a standard double resonance probe, at frequencies of 400.42 MHz (^{1}H), 162.1 MHz (^{31}P) and 100.6 MHz ^{13}C). Samples were packed into 4 mm zirconia rotors and rotated at a magic angle spinning (MAS) rate of 12.5 kHz, except where otherwise stated.

Samples were characterised using standard Bloch decay (BD) and cross-polarisation (CP) MAS techniques (^{1}H π/2 pulse length 2.50 µs, ^{31}P π/2 pulse length 2.55 µs, ^{13}C π/2 pulse length 2.03 µs, ^{1}H-^{13}C CP ^{1}H field strength 77 kHz, ^{1}H-^{13}C CP ^{13}C field strength 55 kHz, ^{1}H-^{13}C CP contact time 1-4 ms, 3 s recycle time for ^{1}H-^{13}C CP and 300 s recycle time for ^{13}C BD, 60 s recycle time for ^{31}P BD (full relaxation was not required as no quantitative analysis of the ^{31}P spectra was performed); SPINAL64 decoupling was used during signal acquisition at ^{1}H field strength 100 kHz. The ^{13}C CP spectrum of OCP-citrate was recorded at 200 K (MAS rate 12 kHz, contact time 2 ms) using the Bruker Avance spectrometer temperature controller unit.

Two versions of the ^{1}H-^{31}P heteronuclear correlation (HETCOR) experiment were performed: one with frequency-switched Lee-Goldburg (FSLG) decoupling during t_1 (^{1}H field strength 100 kHz) and either broadband TPPM decoupling or SPINAL64 decoupling during signal acquisition (typical ^{1}H field strength 87 kHz), and one without FSLG decoupling in t_1 to check the scaling of the frequency scale in the ^{1}H dimension. 64 points were collected in the ^{1}H dimension (f_1) and 512 in the ^{31}P dimension (f_2).

^{13}C $\{^{31}$P$\}$ REDOR measurements were performed at a MAS rate of 12.5 kHz by applying a series of rotor-synchronised ^{31}P π pulses (8.40 µs) separated by the rotor period (80 µs) after the initial ^{1}H-^{13}C CP step, with a ^{13}C refocusing π pulse (9.90 µs) at the midpoint of the ^{31}P pulse train (the length of the pulse train determines the dephasing time).

All solid-state ^{17}O NMR measurements were performed at the UK 850 MHz solid-state NMR Facility with the assistance of Dr Dinu Iuga. ^{17}O DFS MAS spectra were recorded using a standard 4mm low-γ double resonance probe at 115.26 MHz. Samples were packed in a Si_3N_4 rotor and spun at 12.5 kHz (selective π/2 pulse length 8 µs, DFS sweep from 80 to 400 kHz with timing resolution 100 ns and duration 1 ms, 5 s recycle time). Zirconia rotors are unsuitable for investigating calcium phosphate materials, as the spinning sidebands associated with the natural abundance ^{17}O signal at ∼400 ppm interfere with the regions of interest.

Acknowledgements:.

ED acknowledges funding by the Cambridge Commonwealth Trusts (graduate studentship) and a SCI Scholarship. The authors wish to thank Professor Carole Perry for helpful discussions during the preparation of this manuscript. The UK 850 MHz solid-state NMR Facility used in this research was funded by EPSRC and BBSRC, as well as the University of Warwick including via part funding through Birmingham Science City Advanced Materials Projects 1 and 2 supported by Advantage West Midlands (AWM) and the European Regional Development Fund (ERDF).

1. Hu Y-Y, Rawal a, Schmidt-Rohr K (2010) Strongly bound citrate stabilizes the apatite nanocrystals in bone. *Proceedings of the National Academy of Sciences of the United States of America* 107:22425–9.
2. Rey C, Combes C, Drouet C, Glimcher MJ (2009) Bone mineral: update on chemical composition and structure. *Osteoporosis international : a journal established as result of cooperation between the European Foundation for Osteoporosis and the National Osteoporosis Foundation of the USA* 20:1013–21.
3. Dey A et al. (2010) The role of prenucleation clusters in surface-induced calcium phosphate crystallization. *Nature materials* 9:1010–4.
4. Cho G, Wu Y, Ackerman JL (2003) Detection of hydroxyl ions in bone mineral by solid-state NMR spectroscopy. *Science (New York, NY)* 300:1123–7.
5. Wilson EE et al. (2006) Three structural roles for water in bone observed by solid-state NMR. *Biophysical journal* 90:3722–31.
6. Glimcher MJ (2006) Bone: Nature of the Calcium Phosphate Crystals and Cellular, Structural, and Physical Chemical Mechanisms in Their Formation. *Reviews in Mineralogy and Geochemistry* 64:223–282..
7. Akkus O, Adar F, Schaffler MB (2004) Age-related changes in physicochemical properties of mineral crystals are related to impaired mechanical function of cortical bone. *Bone* 34:443–53.
8. Einhorn TA et al. (1988) The mineral and mechanical properties of bone in chronic experimental diabetes. *Journal of Orthopaedic Research* 6:317–323.
9. Yerramshetty JS, Akkus O (2008) The associations between mineral crystallinity and the mechanical properties of human cortical bone. *Bone* 42:476–82.
10. Bala Y et al. (2012) Bone micromechanical properties are compromised during long-term alendronate therapy independently of mineralization. *Journal of bone and mineral research : the official journal of the American Society for Bone and Mineral Research* 27:825–34. Available at: http://www.ncbi.nlm.nih.gov/pubmed/22189833
11. Monma H, Goto M (1983) Succinate-complexed octacalcium phosphate. *Bulletin of the Chemical Society of Japan* 56:3843–3844.
12. Monma H (1984) The incorporation of dicarboxylates into octacalcium bis (hydrogenphosphate) tetrakis (phosphate) pentahydrate. *Bulletin of the Chemical Society of Japan* 57:599–600.
13. Monma H, Goto M (1984) Complexes of Apatitic Layered Compound Ca8(HPO4)2(PO4)4.5H2O with Dicarboxylates. *Journal of Inclusion Phenomena* 2:127–134.
14. Markovic M, Fowler BO, Brown WE (1993) Octacalcium phosphate carboxylates. 2. Characterization and structural considerations. *Chemistry of Materials* 5:1406–1416.
15. Sakamoto K et al. (2008) Synthesis and thermal decomposition of layered calcium phosphates including carboxylate ions. *Thin Solid Films* 517:1354–1357.
16. Fowler BO, Markovic M, Brown WE (1993) Octacalcium phosphate. 3. Infrared and Raman vibrational spectra. *Chemistry of Materials* 5:1417–1423.
17. Sakamoto K et al. (2008) Synthesis and thermal decomposition of layered calcium phosphates including carboxylate ions. *Thin Solid Films* 517:1354–1357.
18. Tsai TWT, Chou F-C, Tseng Y-H, Chan JCC (2010) Solid-state P-31 NMR study of octacalcium phosphate incorporated with succinate. *Physical chemistry chemical physics : PCCP* 12:6692–6697.
19. Clark SJ et al. (2005) First principles methods using CASTEP. *Zeitschrift für Kristallographie* 220:567–570.
20. Gervais C et al. (2004) Combined ab initio computational and experimental multinuclear solid-state magnetic resonance study of phenylphosphonic acid. *Magnetic resonance in chemistry : MRC* 42:445–452.
21. Gao S-P, Pickard CJ, Perlov A, Milman V (2009) Core-level spectroscopy calculation and the plane wave pseudopotential method. *Journal of Physics: Condensed Matter* 21:104203.
22. Markovic M, Fowler BO, Brown WE (1993) Octacalcium phosphate carboxylates. 1. Preparation and identification. *Chemistry of Materials* 5:1401–1405.
23. Tsai TWT, Chou F-C, Tseng Y-H, Chan JCC (2010) Solid-state P-31 NMR study of octacalcium phosphate incorporated with succinate. *Physical chemistry chemical physics : PCCP* 12:6692–7.
24. Yesinowski JP, Eckert H (1987) Hydrogen environments in calcium phosphates: proton MAS NMR at high spinning speeds. *Journal of the American Chemical Society* 109:6274–6282.
25. Davies E, Duer MJ, Ashbrook SE, Griffin JM (2012) Applications of NMR crystallography to problems in biomineralization: refinement of the crystal structure and 31P solid-state NMR spectral assignment of octacalcium phosphate. *Journal of the American Chemical Society* 134:12508–15.
26. Yesinowski JP, Eckert H, Rossman GR (1988) Characterization of hydrous species in minerals by high-speed proton MAS-NMR. *Journal of the American Chemical Society* 110:1367–1375.
27. Cheetham AK, Clayden NJ, Dobson CM, Jakemana RJB (1986) Correlations between 31P N . M . R . Chemical Shifts and Structural Parameters in Crystalline Inorganic phosphates. *J Chem Soc Chem Comm*:195–197.
28. Gorenstein DG, Kar D (1975) ^{31}P chemcial shifts in phosphate diester monoanions. Bond

angle and torsional angle effects. *Biochemical and biophysical research communications* 65:1073–1080.
29. Pickard C, Mauri F (2001) All-electron magnetic response with pseudopotentials: NMR chemical shifts. *Physical Review B* 63:245101.
30. Yates J, Pickard C, Mauri F (2007) Calculation of NMR chemical shifts for extended systems using ultrasoft pseudopotentials. *Physical Review B* 76:024401.
31. Clark SJ et al. (2005) First principles methods using CASTEP. 220:567–570.
32. Hawkes GE, O'Brien P, Salacinski H, Motevalli M, Abrahams I (2001) Solid and Solution State NMR Spectra and the Structure of the Gallium Citrate Complex (NH_4) 3[$Ga(C_6H_5O_7)_2$]· $4H_2O$. *European Journal of Inorganic Chemistry*:1005–1011.
33. Bodor A, Banyai I, Tóth I (2002) 1-H- and 13-C-NMR as tools to study aluminium coordination chemistry: aqueous Al (III) Á citrate complexes. *Coordination Chemistry Reviews* 228:175–186.
34. Wise ER et al. (2007) The Organic−Mineral Interface in Bone Is Predominantly Polysaccharide. *Chemistry of Materials* 19:5055–5057.
35. Hu Y-Y, Rawal a, Schmidt-Rohr K (2010) Strongly bound citrate stabilizes the apatite nanocrystals in bone. *Proceedings of the National Academy of Sciences of the United States of America* 107:22425–9.
36. Nikel O et al. (2012) Solid state NMR investigation of intact human bone quality: balancing issues and insight into the structure at the organic-mineral interface. *The journal of physical chemistry C, Nanomaterials and interfaces* 116:6320–6331.
37. Xu J, Zhu P, Morris MD, Ramamoorthy A (2011) Solid-State NMR Spectroscopy Provides Atomic-Level Insights Into the Dehydration of Cartilage. *The journal of physical chemistry B*.
38. Brown WE, Smith JP, Lehr JR, Frazier AW (1962) Crystallographic and chemical relations between octacalcium phosphate and hydroxyapatite. *Nature* 196:1050–1055.
39. Fernández ME, Zorrilla-Cangas C, García-García R, Ascencio J A, Reyes-Gasga J (2003) New model for the hydroxyapatite–octacalcium phosphate interface. *Acta Crystallographica Section B Structural Science* 59:175–181.
40. Schmidt-Rohr K, Rawal a, Fang X-W (2007) A new NMR method for determining the particle thickness in nanocomposites, using T2, 1H-selective X{1H} recoupling. *The Journal of chemical physics* 126:054701.
41. Kolmas J, Slósarczyk A, Wojtowicz A, Kolodziejski W (2007) Estimation of the specific surface area of apatites in human mineralized tissues using ^{31}P MAS NMR. *Solid state nuclear magnetic resonance* 32:53–8.
42. Maltsev S, Duer MJ, Murray RC, Jaeger C (2007) A solid-state NMR comparison of the mineral structure in bone from diseased joints in the horse. *Journal of Materials Science* 42:8804–8810.
43. Wilson EE et al. (2005) Highly ordered interstitial water observed in bone by nuclear magnetic resonance. *Journal of bone and mineral research : the official journal of the American Society for Bone and Mineral Research* 20:625–34.
44. Arends J et al. (1987) A calcium hydroxide precipitated from aqueous solution: An international multimethod analysis. 84:515–532.
45. Rothwell WP, Waugh JS, Yesinowski JP (1980) High-resolution variable-temperature phosphorus-31 NMR of solid calcium phosphates. *Journal of the American Chemical Society* 102:2637–2643.
46. Aue WP, Roufosse a. H, Glimcher MJ, Griffin RG (1984) Solid-state phosphorus-31 nuclear magnetic resonance studies of synthetic solid phases of calcium phosphate: potential models of bone mineral. *Biochemistry* 23:6110–6114.
47. Carrodegus RG, de Aza S (2011) α-Tricalcium phosphate: synthesis, properties and biomedical applications. *Acta Biomater* 10:3536–3546.